

## Research Article

# Detailed Spectroscopic and Structural Analysis of TiO<sub>2</sub>/WO<sub>3</sub> Composite Semiconductors

**Biborka Boga,<sup>1</sup> István Székely,<sup>2,3</sup> Zsolt Pap,<sup>2,3,4</sup> Lucian Baia ,<sup>2,3</sup> and Monica Baia ,<sup>2,3</sup>**

<sup>1</sup>Faculty of Chemistry and Chemical Engineering, Babeş-Bolyai University, Arany János 11, Cluj-Napoca 400028, Romania

<sup>2</sup>Nanostructured Materials and Bio-Nano-Interfaces Center, Institute for Interdisciplinary Research on Bio-Nano-Sciences, Treboniu Laurian 42, Cluj-Napoca 400271, Romania

<sup>3</sup>Faculty of Physics, Babeş-Bolyai University, Mihail Kogălniceanu 1, Cluj-Napoca 400084, Romania

<sup>4</sup>Institute of Environmental Science and Technology, Tisza Lajos krt. 103, Szeged 6720, Hungary

Correspondence should be addressed to Lucian Baia; [lucian.baia@phys.ubbcluj.ro](mailto:lucian.baia@phys.ubbcluj.ro)

Received 15 March 2018; Accepted 4 September 2018; Published 2 October 2018

Academic Editor: Vincenza Crupi

Copyright © 2018 Biborka Boga et al. This is an open access article distributed under the Creative Commons Attribution License, which permits unrestricted use, distribution, and reproduction in any medium, provided the original work is properly cited.

WO<sub>3</sub>-TiO<sub>2</sub> composite materials were obtained using commercial titania (Evonik Aeroxide P25) and hydrothermally crystallized WO<sub>3</sub>. Different ratios of TiO<sub>2</sub>/WO<sub>3</sub> were investigated, starting at 1 wt.% of WO<sub>3</sub> to 50 wt.%. The morphology of WO<sub>3</sub> was of the star-like type, and its structure is basically composed of monoclinic crystalline phase. All spectroscopic characteristics of the composites and their derived data (band-gap energy value, light absorption threshold, and IR specific bands) directly varied with the increase of the WO<sub>3</sub> content. However, the oxalic acid photodegradation achieved under UV light reached the highest yield for 24 wt.% WO<sub>3</sub> content, a result that was attributed to the charge separation efficiency and the surface hydrophilicity. The latter mentioned reason points out the crucial importance of the surface quality of the investigated structure in photocatalytic tests.

## 1. Introduction

The study of semiconductors remained in the last years a systematically investigated research topic. The implementation of nanomaterials in the industry had a major role in the blooming research of nanomaterials. One of these nanomaterials is tungsten trioxide (WO<sub>3</sub>), a transition metal oxide with large applicability spectra that is commonly used in paints as pigment [1], in solar cells for electricity production [2, 3], and in coatings for heat production from absorbing solar energy [4], such as humidity, moisture, and gas sensors [5–7]. This oxide is also an important component in “smart windows” due to its electrochromic properties [8]. Moreover, WO<sub>3</sub> is used as a catalytic and photocatalytic purifier for air and water [9, 10].

WO<sub>3</sub> nanomaterials (nano- or microcrystals) can be synthesized via various methods, such as hydrothermal crystallization [11], solvothermal crystallization [12], chemical vapor deposition [13], atomic layer deposition [14], physical vapor deposition [15], sol-gel synthesis [16], and laser pyrolysis [17]. There is an extensive list of possibilities

towards WO<sub>3</sub> production, but the most widely used technique is the hydrothermal crystallization because this method is relatively simple, and it is not expensive and time-consuming [18–21].

Tungsten trioxide has an interesting peculiarity; in certain cases, it can act as a charge separator [22]. Due to this feature, it is a viable component for binary composite systems, in which another metal oxide is used as an electron donor, generally TiO<sub>2</sub> [23] or ZnO [24], but NiO [25] was also used. The final goal of these composite systems is either to apply them as a sensor or as a photocatalyst, or even both simultaneously. Photocatalytic efficiency of WO<sub>3</sub> semiconductor can be enhanced if noble metals are added, WO<sub>3</sub>/Au, WO<sub>3</sub>/Ag, or WO<sub>3</sub>/Pt composite systems being related to show an improved photocatalytic efficiency towards the removal of organic pollutants in comparison with commercial TiO<sub>2</sub> (Evonik Aeroxide P25) [26–28]. The photocatalytic activity of ternary composites based on WO<sub>3</sub>, commercial TiO<sub>2</sub>, and noble metals (WO<sub>3</sub>/TiO<sub>2</sub>/noble metals) was also intensively studied [29–31]. The most commonly used methods for the preparation of WO<sub>3</sub>/P25

composites are the mechanical mixing or the adjustment of the semiconductors' surface charge, and in both cases, the composites photocatalytic efficiency was improved as compared to that exhibited by P25 [32, 33].

In this study, tungsten trioxide microcrystals were synthesized via hydrothermal crystallization, and their spectroscopic and structural features were investigated. Various weight percentage composites based on the synthesized  $\text{WO}_3$  and commercial  $\text{TiO}_2$  (Evonik Aeroxide P25) were prepared by mechanical mixing method, and the photocatalytic activity of these binary composite systems was assessed.

## 2. Experimental

**2.1. Chemicals.** The chemicals employed for the synthesis of  $\text{WO}_3$  microcrystals were ammonium metatungstate hydrate ( $(\text{NH}_4)_6\text{H}_2\text{W}_{12}\text{O}_{40}\cdot x\text{H}_2\text{O}$ , Sigma-Aldrich, 99.99%) and hydrochloric acid (HCl, NORDIC 37%, 12 M). The photocatalytic activity was evaluated in the aqueous solution (3 mM) of oxalic acid-OA ( $\text{HO}_2\text{C}-\text{CO}_2\text{H}\cdot 2\text{H}_2\text{O}$ , Sigma-Aldrich, 98%). Commercial  $\text{TiO}_2$  (Evonik Aeroxide P25) was used for the  $\text{WO}_3/\text{TiO}_2$  composites preparation. All chemicals were used as received without further modification or purification.

**2.2. Synthesis of Star-Like  $\text{WO}_3$  Microcrystals.** 1.23 g of ammonium metatungstate hydrate (AMT) was dissolved in 20 mL of water under constant stirring. 0.84 mL (12 M) hydrochloric acid (HCl) was added to the solution which was stirred for 15 minutes at room temperature. A yellow suspension was obtained after the hydrothermal crystallization, which was carried out at 180°C for 4 hours. After the autoclave cooled down at room temperature, the product was centrifuged ( $3 \times 15$  minutes, 1600 rpm) and washed with deionized water in order to remove the impurities remained in the product. The product was dried at 70°C for 6 hours and annealed at 500°C for 30 minutes (heating rate  $5^\circ\text{C}\cdot\text{min}^{-1}$ ) [34]. The  $\text{WO}_3$ -AMT abbreviation was further used to identify the  $\text{WO}_3$  crystals synthesized from ammonium metatungstate hydrate.

**2.3. The Preparation of  $\text{TiO}_2/\text{WO}_3$  Composites.** The  $\text{TiO}_2/\text{WO}_3$  composites were obtained via mechanical mixing ( $3 \times 5$  minutes), by using the physical mixing method. 50–50, 67–33, 76–24, 90–10, and 99–1 wt.%  $\text{TiO}_2/\text{WO}_3$  composites were prepared and investigated. According to our previous work [29], no structural or morphological changes were observed for the two components, when mixing them by using the above-described approach.

**2.4. Characterization Methods.** The assessment of the crystalline structure of the composite components was carried out by the means of X-Ray Diffraction (XRD) measurements. The XRD diffractograms were recorded on a Shimadzu 6000 diffractometer (Shimadzu Corporation, Kyoto, Japan), by using  $\text{Cu-K}\alpha$  irradiation, ( $\lambda = 1.5406 \text{ \AA}$ ). The crystalline

phases of the semiconductors were evaluated and the crystallites' average size was calculated by using the Scherrer equation [35], whereas the anatase/rutile ratios in P25 were evaluated by the well-known Banfield approach [36].

Diffuse reflectance spectroscopy (DRS) measurements were performed by using the JASCO-V650 spectrophotometer ( $\lambda = 250 - 800 \text{ nm}$ ) equipped with ILV-724 integration sphere. The band-gap energy of the composites system was determined using the following equation [37–39]:

$$(E) = \frac{h \cdot c}{\lambda}, \quad (1)$$

where  $(E)$  is the band-gap energy,  $h$  is Plank constant,  $c$  is the speed of light  $= 3.0 \times 10^8 \text{ m}\cdot\text{sec}^{-1}$ , and  $\lambda$  is the cut-off wavelength.

A JASCO 4100 (Jasco, Tokyo, Japan) spectrometer was used to record the IR spectra of the composites, at room temperature, in the spectral range of  $400\text{--}4000 \text{ cm}^{-1}$ , with a spectral resolution of  $4 \text{ cm}^{-1}$ . The samples were prepared in the form of KBr pellets.

The SEM micrographs were recorded by using an FEI Quanta 3D FEG scanning electron microscope operating at an accelerating voltage of 25 kV. The  $\text{WO}_3$  nanomaterials were covered with Au to amplify the secondary electron signal, while the morphological peculiarities of the semiconductor were uncovered.

The investigation of photocatalytic performance was carried out in the presence of  $2 \times 60 \text{ W}$  fluorescence UV lamps with  $\lambda \approx 365 \text{ nm}$  emission maximum, under vigorous stirring ( $C_{\text{suspension}} = 1 \text{ g}\cdot\text{L}^{-1}$ ;  $V_{\text{suspension}} = 75 \text{ mL}$ ;  $C_{\text{oxalic acid}} = 3 \text{ mM}$ ). The photocatalytic degradation was followed for 3 hours using high-performance liquid chromatography (HPLC). The measurements were carried out by using Merck-Hitachi type D-7000 chromatograph equipped with an L-4250 UV-Vis detector. The volume of the loop was  $20 \mu\text{L}$  and the chromatography column was installed with Grom Resin ZH-type load. The eluent was 0.06%  $\text{H}_2\text{SO}_4$  aqueous solution, and the applied flow rate was  $0.8 \text{ mL}\cdot\text{min}^{-1}$ . The key parameters investigated here were the conversion (X) and the reaction rate.

## 3. Results and Discussion

**3.1. Crystalline Structure and Particle Size of the Semiconductors.** The first step in the investigation series was to check the quality of the composite components. From the XRD patterns (Figure 1), the crystalline phase and the mean primary particle size of the synthesized semiconductors were established. In the case of  $\text{WO}_3$ , only the monoclinic crystalline phase was detected, as it can be seen from the diffractogram. However, based on our previous work [33], one can infer that this synthesis procedure gives rise to hierarchical structures made up from fine micrometric needle crystals (30–50 nm wide and 3–4  $\mu\text{m}$  long) that form a star-like shaped structure (therefore the Scherrer equation was not used). The particle size of the  $\text{WO}_3$  stars was between 3 and 4  $\mu\text{m}$  (as described in Section 3.3). Regarding the commercial  $\text{TiO}_2$ , both anatase and rutile crystalline phases were observed, the ratio between anatase and rutile was

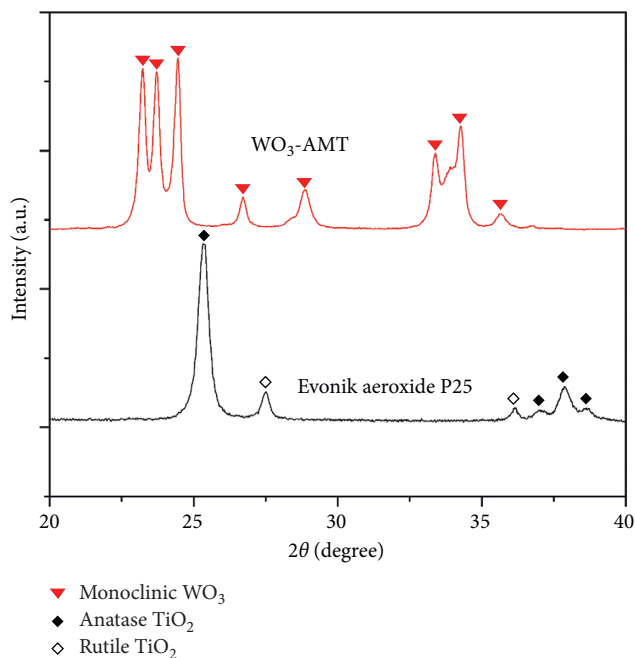


FIGURE 1: XRD patterns of monoclinic  $\text{WO}_3$  and commercial  $\text{TiO}_2$ , the two components of the obtained composites.

estimated (89:11), and the primary calculated particle size (25–40 nm) was very close to the values reported in the literature.

### 3.2. Optical Properties of the Prepared Composite System.

As the composite structure contains both oxides, it was crucial to investigate the optical properties of these materials (Figure 2). The band-gap energy values were determined by using the light absorption threshold method, as mentioned in Section 2.4. In the case of the  $\text{WO}_3$ -AMT semiconductor, the light absorption threshold was found to be around 550 nm and the calculated band-gap energy was of  $\approx 2.25$  eV, but it should be kept in mind that the band-gap energy value of the commercial  $\text{TiO}_2$  is  $\approx 3.2$  eV [33]. Concerning the composites, the light absorption thresholds and the band-gap energy values were as follows: 394 nm,  $\approx 3.14$  eV (99-1 wt.% P25- $\text{WO}_3$ ); 414 nm,  $\approx 2.99$  eV (90-10 wt.% P25- $\text{WO}_3$ ); 449 nm,  $\approx 2.76$  eV (76-24 wt.% P25- $\text{WO}_3$ ); 447 nm,  $\approx 2.77$  eV (67-33 wt.% P25- $\text{WO}_3$ ); and 451 nm,  $\approx 2.74$  eV (50-50 wt.% P25- $\text{WO}_3$ ). The lowest band-gap energy was found for the 50-50 wt.% P25- $\text{WO}_3$  composite. One observes that the  $\text{WO}_3$  amount has a significant effect on the band-gap energy value, and a very interesting fact is that even 1% of monoclinic tungsten trioxide can influence it, by slightly reducing this value by 0.06 eV. By adding 10%  $\text{WO}_3$  to the composite composition, the band-gap energy was found to further decrease by 0.21 eV. By increasing the amount of  $\text{WO}_3$  to 24%, the band-gap energy was lowered by 0.44 eV. According to these results, the 99-1% wt.% P25- $\text{WO}_3$  and 90-10% wt.% P25- $\text{WO}_3$  composites should act as photocatalysts under UV light irradiation, while the 76-24% wt.% P25- $\text{WO}_3$ , 67-33% wt.% P25- $\text{WO}_3$ , and 50-50% wt.% P25-

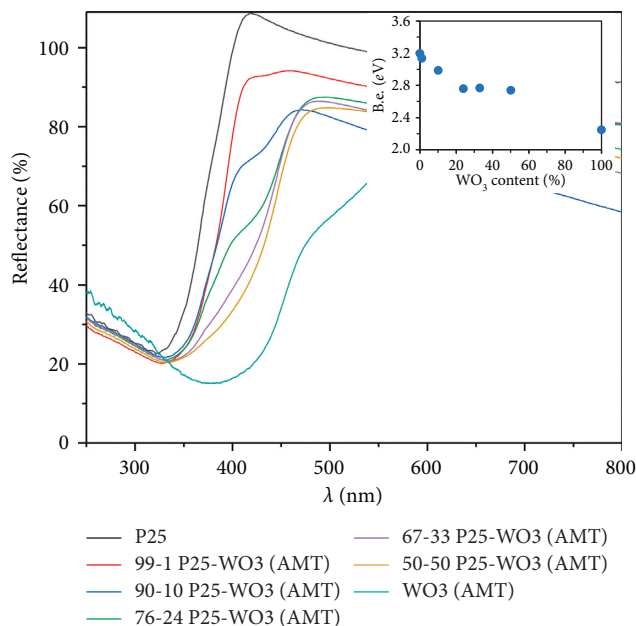


FIGURE 2: The reflectance spectra of the prepared  $\text{WO}_3/\text{TiO}_2$  composites system and the band-gap energy dependence on the  $\text{WO}_3$  content (inset figure).

$\text{WO}_3$  composites may have photocatalytic potential under visible light irradiation.

### 3.3. Morphological Features of the Synthesized Semiconductor.

SEM measurements revealed that the morphology of the  $\text{WO}_3$  ( $\text{WO}_3$ -AMT) microcrystals synthesized from ammonium metatungstate hydrate was of star-like type (Figure 3). The diameter of the stars was between 3 and 4  $\mu\text{m}$ , each star being constructed from microfibers of 3–4  $\mu\text{m}$  length. More importantly, it was found that all the microstars showed the same structure and morphology (i.e., high monodispersity), which can reinforce all the conclusions derived from the study.

### 3.4. FT-IR Characterization of the Prepared Composites System.

By analyzing the IR spectra (Figure 4) of the obtained composites, the specific signals of  $\text{TiO}_2$  were detected without any special changing trends, excepting the alteration of some signals proportionally with the composite components' ratio. The main spectral feature associated with titania was the large band between 400 and 700  $\text{cm}^{-1}$ , which can be attributed to the stretching vibrations of Ti-O-Ti and Ti-O bonds. In the case of  $\text{WO}_3$ , several specific spectral characteristics were observed, such as the ones between 600 and 1000  $\text{cm}^{-1}$  (the most intense one being located at 931  $\text{cm}^{-1}$ ), which were assigned to different W-O-W stretching modes. The small but distinct band at 1035  $\text{cm}^{-1}$  was given by the stretching vibration of the W=O bonds [40]. These signals involving tungsten bond vibrations were also dependent on the  $\text{WO}_3$  concentration. The band at 1390  $\text{cm}^{-1}$  was interestingly found to be given by  $\text{NH}_4^+$  ions [41]. At the first view, this is rather surprising; but actually, it can be considered an expected appearance having in view that  $\text{WO}_3$  was obtained by using

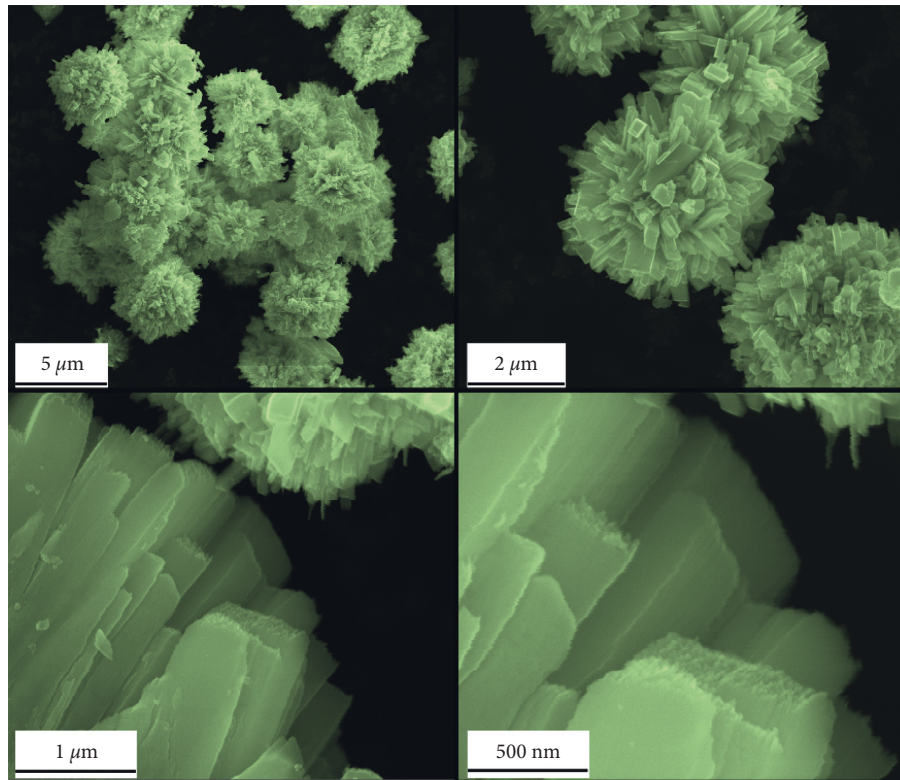


FIGURE 3: SEM micrographs of the  $\text{WO}_3$ -AMT semiconductors, showing the star-like shape and a fine hierarchical structure.

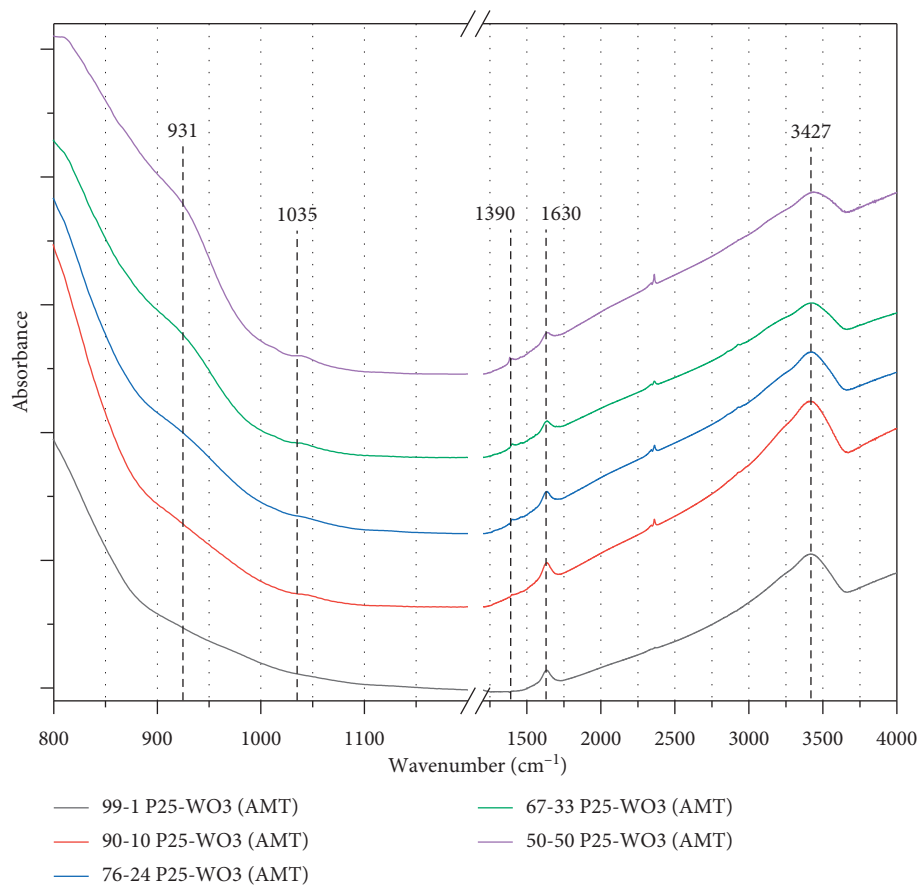


FIGURE 4: Infrared spectra of the prepared  $\text{WO}_3/\text{TiO}_2$  composite system.



ammonium metatungstate. The only bands that differently changed self-dependent on the  $\text{WO}_3$  content were those directly related to the surface hydrophilicity, namely, those at  $1630$  and  $3427\text{ cm}^{-1}$  assigned to OH vibrations. These bands exhibit a relatively high intensity for the samples with  $\geq 24$  wt.%  $\text{WO}_3$  and a slow decrease of it for smaller  $\text{WO}_3$  content. This result points out the high water affinity of 90-10 wt.% P25- $\text{WO}_3$  and 76-24 wt.% P25- $\text{WO}_3$ , which could have an impact on the photoactivity of these materials.

**3.5. Photocatalytic Activity.** The evaluation of the photocatalytic performance was carried out by analyzing the oxalic acid degradation curves, which provide qualitative and quantitative information (Figure 5). The photocatalytic performance was quantitatively described by using the conversion values (X).

No photocatalytic activity was observed when bare  $\text{WO}_3$  and 50-50 wt.%  $\text{TiO}_2/\text{WO}_3$  were used as photocatalysts in 3 mM oxalic acid solution. This photocatalytic inefficiency of bare  $\text{WO}_3$  could be due to the  $\text{WO}_3$  particles dimension, which is relatively high ( $3\text{--}4\ \mu\text{m}$ ). In the case of 50-50 wt.%  $\text{TiO}_2/\text{WO}_3$  composite, the reason could be the screening effect of the  $\text{WO}_3$  crystals on the  $\text{TiO}_2$  particles so that the system had a deficiency being activated under UV light irradiation. In this case, the generation of charge carriers was decreased, and consequently, the photocatalytic activity was low in the composites with high  $\text{WO}_3$  content. Only 28% of oxalic acid was removed using the 67-33 wt.%  $\text{TiO}_2/\text{WO}_3$  composite system in contrast to 76-24 wt.%  $\text{TiO}_2/\text{WO}_3$  system, where 99% conversion was achieved. 68% conversion was obtained in the case of 90-10 wt.%  $\text{TiO}_2/\text{WO}_3$  composites and 95% conversion rate was observed for the 99-1 wt.%  $\text{TiO}_2/\text{WO}_3$  composites. The reference catalyst (commercial  $\text{TiO}_2$ ) degraded 73.3 wt.% of oxalic acid.

The most efficient composite for oxalic acid degradation was the 76-24 wt.%  $\text{TiO}_2/\text{WO}_3$  system because the recombination process was inhibited successfully so that the separation of the charge carriers was the most efficient in the case of this sample. The first five points were taken into consideration for the calculation of the initial reaction rates. The concentration changes of oxalic acid (at 0, 15, 30, 45, and 60 min) were plotted versus time to determine the initial reaction rate ( $r_i$ ) values. The linearization of these two parameters and its slope gave the initial reaction rate values. The initial reaction rate of the bare  $\text{WO}_3$  and of 50-50 wt.%  $\text{TiO}_2\text{-WO}_3$  composites were null because these systems were not photoactive. In the other cases, the reaction rate was  $5.80\text{ mM}\cdot\text{s}^{-1}\cdot 10^{-3}$  (67-33%),  $22.10\text{ mM}\cdot\text{s}^{-1}\cdot 10^{-3}$  (76-24%),  $12.90\text{ mM}\cdot\text{s}^{-1}\cdot 10^{-3}$  (90-10%),  $11.40\text{ mM}\cdot\text{s}^{-1}\cdot 10^{-3}$  (99-1%), and  $12.7\text{ mM}\cdot\text{s}^{-1}\cdot 10^{-3}$  (in the case of commercial  $\text{TiO}_2$ ). The conversion, initial reaction rate, and band-gap energy values are summarized in Table 1.

All the activity-related parameters clearly show that it must be a specific parameter responsible for the high photoactivity. The band-gap energy values of the composites can be eliminated as the main reason because it is a parameter that varied concomitantly with the  $\text{WO}_3$  content. As no structural and morphological changes occurred during

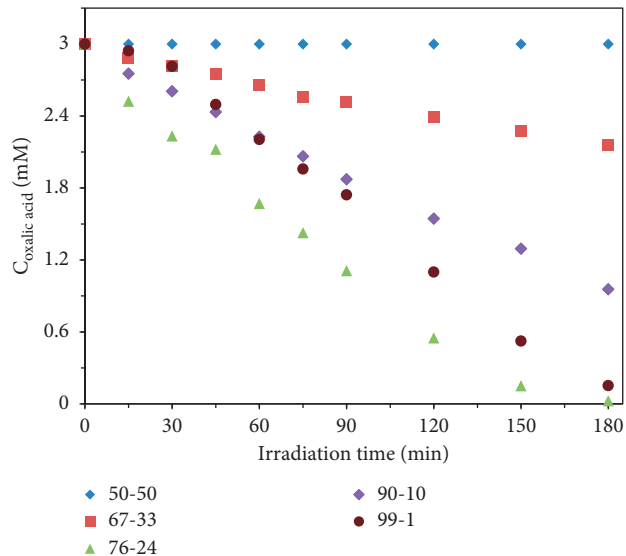


FIGURE 5: Photodegradation of 3 mM oxalic acid using under UV light irradiation in the presence of 50-50, 67-33, 76-24, 90-10, and 99-1 wt.%  $\text{TiO}_2/\text{WO}_3$  composites.

TABLE 1: Summary of the photocatalytic properties for the various composite system and reference catalysts.

Samples	X—conversion (%) (after 3 hours)	$r_i$ ( $\text{mM}\cdot\text{second}^{-1}\cdot 10^{-3}$ )	Band-gap energy value (eV)
$\text{WO}_3$ (AMT)	0.0	0.0	2.25
P25	73.3	12.7	3.20
50% P25-50% $\text{WO}_3$ (AMT)	0.0	0.0	2.74
67% P25-33% $\text{WO}_3$ (AMT)	28.0	05.8	2.77
76% P25-24% $\text{WO}_3$ (AMT)	<b>99.0</b>	<b>22.1</b>	<b>2.76</b>
90% P25-10% $\text{WO}_3$ (AMT)	68.0	12.9	2.99
99% P25-1% $\text{WO}_3$ (AMT)	95.0	11.4	3.14

the composite preparation, other approaches should be exploited. Firstly, an analog case can be involved, in which a similar phenomenon was explained [29]. As the amount of  $\text{WO}_3$  increases, so does the charge separation efficiency in the composites. However, after a specific concentration of  $\text{WO}_3$ , this was detrimental, because the  $\text{WO}_3$  itself is not photoactive. This means that increasing too much the ratio of a charge separator (without self-activity), a lowering of the overall photoactivity occurs. However, this approach may be not sufficient alone. The intensity of the IR bands at  $1630\text{ cm}^{-1}$  and  $3427\text{ cm}^{-1}$  showed nearly the same trend as the photoactivity. This means that the photocatalytic degradation is in direct relationship with the hydrophilicity of the photocatalyst (a fact well-known for  $\text{TiO}_2$  [42]), which was confirmed here for the first time in case of  $\text{TiO}_2\text{-WO}_3$  composites.

## 4. Conclusions

In the herein presented study, WO<sub>3</sub>-TiO<sub>2</sub> composites with different TiO<sub>2</sub>/WO<sub>3</sub> ratios (1 wt.% of WO<sub>3</sub> to 50 wt.%) were obtained by using commercial titania (Evonik Aeroxide P25) and hydrothermally crystallized WO<sub>3</sub>. The morphology of the synthesized hierarchical WO<sub>3</sub> semiconductors was star-like shaped with a diameter between 3 and 4 μm, and WO<sub>3</sub>'s determined crystal phase was monoclinic. The present study proves that WO<sub>3</sub> microcrystals of relatively large dimension, without photoactivity, can improve the photocatalytic efficiency of the commercial TiO<sub>2</sub>, acting as a charge separator. The band-gap energy values of the composites were found to be dependent on the WO<sub>3</sub> content as well, but no correlation was established with the photoactivity.

The 76-24 wt.% TiO<sub>2</sub>/WO<sub>3</sub> composite system has shown the highest photocatalytic activity, reaching a conversion rate of 99%. Also, this sample and the one with 10 wt.% of WO<sub>3</sub> exhibited the most intense water affinity as revealed by the IR bands assigned to water vibrations, showing a clear correlation between these structural entities and photoactivity.

The obtained results from this study also suggest that these composites system could be used as efficient photocatalysts for other pollutants removal (methyl orange and salicylic acid), gas sensors, and sensors for detection of organic pollutants containing the carboxylic functional group or could be even used for ternary WO<sub>3</sub>/TiO<sub>2</sub>/noble metal composites.

## Data Availability

All the data shown throughout the five figures and one table used to support the findings of this study are included within the article.

## Conflicts of Interest

The mentioned received funding did not lead to any conflicts of interest regarding the publication of this manuscript. Furthermore, the authors do not have any other conflicts of interest, concerning the present work.

## Authors' Contributions

Biborka Boga and István Székely contributed equally to this work.

## Acknowledgments

Biborka Boga would like to thank the Hungarian Ministry of Economic and Foreign Affairs for the scholarship "Márton Áron" Programme for Gifted Youngsters. István Székely acknowledges the funding provided by the Collegium Talentum scholarship supported by the Sapientia Hungariae Foundation. Biborka Boga, István Székely, and Zsolt Pap would like to express their gratitude towards the "RING 2017," EFOP-3.6.2-16-2017-00010 project, funded by the European Union and the Government of Hungary. In addition, the authors would like to thank Dr. Klára Magyari

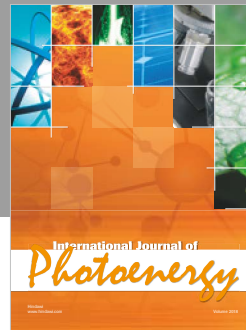
for recording the IR spectra and Zsejke-Réka Tóth for the photocatalytic tests.

## References

- [1] P. Patnaik, *Handbook of Inorganic Chemicals*, McGraw-Hill, New York, NY, USA, 2003.
- [2] M. Gómez, J. Lu, E. Olsson, A. Hagfeldt, and C. Granqvist, "High efficiency dye-sensitized nanocrystalline solar cells based on sputter deposited Ti oxide films," *Solar Energy Materials and Solar Cells*, vol. 64, no. 1, pp. 385–392, 2000.
- [3] T. Lindgren, J. M. Mwabora, E. Avendano et al., "Photoelectrochemical and optical properties of nitrogen doped titanium dioxide films prepared by reactive DC magnetron sputtering," *Journal of Physical Chemistry B*, vol. 107, no. 24, pp. 5709–5716, 2003.
- [4] P. C. Lansåker, P. Petersson, G. A. Niklasson, and C. G. Granqvist, "Thin sputter deposited gold films on In<sub>2</sub>O<sub>3</sub>:Sn, SnO<sub>2</sub>:In, TiO<sub>2</sub> and glass: optical, electrical and structural effects," *Solar Energy Materials and Solar Cells*, vol. 117, pp. 462–470, 2013.
- [5] A. Tripathi, V. Tripathi, N. K. Pandey, and K. Tiwari, "Resistive type moisture sensor based on WO<sub>3</sub> nanomaterial," *Sensors and Transducers*, vol. 143, pp. 152–161, 2012.
- [6] J. L. Solis, A. Hoel, L. B. Kish, C. G. Granqvist, S. Saukko, and V. Lantto, "Gas-sensing properties of nanocrystalline WO<sub>3</sub> films made by advanced reactive gas deposition," *Journal of the American Ceramic Society*, vol. 84, no. 7, pp. 1504–1508, 2001.
- [7] K. Galatsis, Y. X. Li, W. Wlodarski et al., "Comparison of single and binary oxide MoO<sub>3</sub>, TiO<sub>2</sub> and WO<sub>3</sub> sol-gel gas sensors," *Sensors and Actuators B: Chemical*, vol. 83, no. 1–3, pp. 276–280, 2002.
- [8] E. Lassner and W. Schubert, *Tungsten: properties, chemistry, technology of the elements, alloys, and chemical compounds*, Springer, Berlin, Germany, 1999.
- [9] A. Amoozadeh and S. Rahmani, "Nano-WO<sub>3</sub>-supported sulfonic acid: New, efficient and high reusable heterogeneous nano catalyst," *Journal of Molecular Catalysis A: Chemical*, vol. 396, pp. 96–107, 2015.
- [10] K. Sayama, H. Hayashi, T. Arai, M. Yanagida, T. Gunji, and H. Sugihara, "Highly active WO<sub>3</sub> semiconductor photocatalyst prepared from amorphous peroxy-tungstic acid for the degradation of various organic compounds," *Applied Catalysis B: Environmental*, vol. 94, no. 1–2, pp. 150–157, 2010.
- [11] S. Cao, C. Zhao, T. Han, and L. Peng, "Hydrothermal synthesis, characterization and gas sensing properties of the WO<sub>3</sub> nanofibers," *Materials Letters*, vol. 169, pp. 17–20, 2016.
- [12] Z. Wang, M. Hu, and Y. Qin, "Solvothermal synthesis of WO<sub>3</sub> nanocrystals with nanosheet and nanorod morphologies and the gas-sensing properties," *Materials Letters*, vol. 171, pp. 146–149, 2016.
- [13] N. Shankar, M. F. Yu, S. P. Vanka, and N. G. Glumac, "Synthesis of tungsten oxide (WO<sub>3</sub>) nanorods using carbon nanotubes as templates by hot filament chemical vapor deposition," *Materials Letters*, vol. 60, no. 6, pp. 771–774, 2006.
- [14] I. M. Szilágyi, E. Santala, M. Heikkilä et al., "Photocatalytic properties of WO<sub>3</sub>/TiO<sub>2</sub> core/shell nanofibers prepared by electrospinning and atomic layer deposition," *Chemical Vapor Deposition*, vol. 19, no. 4–6, pp. 149–155, 2013.
- [15] Y. B. Li, Y. Bando, D. Golberg, and K. Kurashima, "WO<sub>3</sub> nanorods/nanobelts synthesized via physical vapor deposition process," *Chemical Physics Letters*, vol. 367, no. 1–2, pp. 214–218, 2003.

- [16] T. Yang, Y. Zhang, and C. Li, "Large scale production of spherical  $\text{WO}_3$  powder with ultrasonic spray pyrolysis assisted by sol-gel method for hydrogen detection," *Ceramics International*, vol. 40, no. 1, pp. 1765–1769, 2014.
- [17] M. Govender, L. Shikwambana, B. W. Mwakikunga, E. Sideras-Haddad, R. M. Erasmus, and A. Forbes, "Esopen access formation of tungsten oxide nanostructures by laser pyrolysis: Stars, fibers, and spheres," *Nanoscale Research Letters*, vol. 6, no. 1, p. 166, 2011.
- [18] M. Ahmadi, R. Younesi, and M. J. F. Guinel, "Synthesis of tungsten oxide nanoparticles using a hydrothermal method at ambient pressure," *Journal of Materials Research*, vol. 29, no. 13, pp. 1424–1430, 2014.
- [19] S. Bai, K. Zhang, R. Luo, D. Li, A. Chen, and C.C. Liu, "Low-temperature hydrothermal synthesis of  $\text{WO}_3$  nanorods and their sensing properties for  $\text{NO}_2$ ," *Journal of Materials Chemistry*, vol. 22, no. 25, p. 12643, 2012.
- [20] D. J. Ham, A. Phuruangrat, S. Thongtem, and J. S. Lee, "Hydrothermal synthesis of monoclinic  $\text{WO}_3$  nanoplates and nanorods used as an electrocatalyst for hydrogen evolution reactions from water," *Chemical Engineering Journal*, vol. 165, no. 1, pp. 365–369, 2010.
- [21] S. S. Shendage, V. L. Patil, S. A. Vanalakar et al., "Sensitive and selective  $\{\text{NO}_2\}$  gas sensor based on  $\{\text{WO}_3\}$  nanoplates," *Sensors and Actuators B: Chemica*, vol. 240, pp. 426–433, 2017.
- [22] K. Tennakone, O. A. Ileperuma, J. M. S. Bandara, and W. C. B. Kiridena, " $\text{TiO}_2$  and  $\text{WO}_3$  semiconductor particles in contact: photochemical reduction of  $\text{WO}_3$  to the non-stoichiometric blue form," *Semiconductor Science and Technology*, vol. 7, no. 3, pp. 423–424, 1992.
- [23] B. Tryba, M. Piszcz, and A. W. Morawski, "Photocatalytic Activity of  $\text{TiO}_2/\text{WO}_3$  Composites," *International Journal of Photoenergy*, vol. 2009, Article ID 297319, 7 pages, 2009.
- [24] J. Xie, Z. Zhou, Y. Lian et al., "Simple preparation of  $\text{WO}_3$ -ZnO composites with UV-Vis photocatalytic activity and energy storage ability," *Ceramics International*, vol. 40, no. 8, pp. 12519–12524, 2014.
- [25] M. Bao, Y. Chen, F. Li et al., "Plate-like p-n heterogeneous  $\text{NiO}/\text{WO}_3$  nanocomposites for high-performance room temperature  $\text{NO}_2$  sensors," *Nanoscale*, vol. 6, no. 8, p. 4063, 2014.
- [26] D. P. Depuccio, P. Botella, B. O'Rourke, and C. C. Landry, "Degradation of methylene blue using porous  $\text{WO}_3$ ,  $\text{SiO}_2$ - $\text{WO}_3$ , and their Au-loaded analogs: Adsorption and photocatalytic studies," *ACS Applied Materials and Interfaces*, vol. 7, no. 3, pp. 1987–1996, 2015.
- [27] W. Zhu, J. Liu, S. Yu, Y. Zhou, and X. Yan, "Ag loaded  $\text{WO}_3$  nanoplates for efficient photocatalytic degradation of sulfanilamide and their bactericidal effect under visible light irradiation," *Journal of Hazardous Materials*, vol. 318, pp. 407–416, 2016.
- [28] Z. Wen, W. Wu, Z. Liu, H. Zhang, J. Li, and J. Chen, "Ultrahigh-efficiency photocatalysts based on mesoporous Pt- $\text{WO}_3$  nano hybrids," *Physical Chemistry Chemical Physics*, vol. 15, no. 18, p. 6773, 2013.
- [29] É. Karácsanyi, L. Baia, A. Dombi et al., "The photocatalytic activity of  $\text{TiO}_2/\text{WO}_3$ /noble metal (Au or Pt) nano-architectures obtained by selective photodeposition," *Catalysis Today*, vol. 208, pp. 19–27, 2013.
- [30] M. Rusu, M. Baia, Zs. Pap, V. Danciu, and L. Baia, "Structural investigations of  $\text{TiO}_2$ - $\text{WO}_3$ -Au porous composites," *Journal of Molecular Structure*, vol. 1073, pp. 150–156, 2014.
- [31] G. Kovács, L. Baia, A. Vulpoi et al., " $\text{TiO}_2/\text{WO}_3/\text{Au}$  nano-architectures' photocatalytic activity, "from degradation intermediates to catalysts' structural peculiarities", part I: Aerioxide P25 based composites," *Applied Catalysis B: Environmental*, vol. 147, pp. 508–517, 2014.
- [32] L. Baia, E. Orbán, S. Fodor et al., "Preparation of  $\text{TiO}_2/\text{WO}_3$  composite photocatalysts by the adjustment of the semiconductors' surface charge," *Materials Science in Semiconductor Processing*, vol. 42, pp. 66–71, 2016.
- [33] I. Székely, G. Kovács, L. Baia, V. Danciu, and Zs. Pap, "Synthesis of shape-tailored  $\text{WO}_3$  micro-/nanocrystals and the photocatalytic activity of  $\text{WO}_3/\text{TiO}_2$  composites," *Materials*, vol. 9, no. 4, p. 258, 2016.
- [34] S. K. Biswas and J. O. Baeg, "A facile one-step synthesis of single crystalline hierarchical  $\text{WO}_3$  with enhanced activity for photoelectrochemical solar water oxidation," *International Journal of Hydrogen Energy*, vol. 38, no. 8, pp. 3177–3188, 2013.
- [35] R. Jenkins and R. Snyder, *Introduction to Powder Diffraction*, John Wiley & Sons, New York, NY, USA, 1996.
- [36] H. Zhang and J. F. Banfield, "Understanding polymorphic phase transformation behavior during growth of nanocrystalline aggregates: insights from  $\text{TiO}_2$ ," *Journal of Physical Chemistry B*, vol. 104, no. 15, pp. 3481–3487, 2000.
- [37] M. R. Hoffmann, S. T. Martin, W. Choi, and D. W. Bahnemann, "Environmental Applications of Semiconductor Photocatalysis," *Chemical Reviews*, vol. 95, no. 1, pp. 69–96, 1995.
- [38] S. S. Srinivasan, N. Kislov, J. Wade, M. T. Smith, E. K. Stefanakos, and Y. Goswami, "Mechanochemical synthesis, structural characterization and visible light photocatalysis of  $\text{TiO}_2/\text{ZnFe}_2\text{O}_4$  nanocomposites," in *Proceedings of Symposium Materials Research Society*, December 2005.
- [39] S. S. Srinivasan, J. Wade, and E. K. Stefanakos, "Synthesis and Characterization of Photocatalytic  $\text{TiO}_2$ - $\text{ZnFe}_2\text{O}_4$  Nanoparticles," *Journal of Nanomaterials*, vol. 2006, Article ID 45712, 4 pages, 2006.
- [40] H. I. S. Nogueira, A. M. V. Cavaleiro, J. Rocha, T. Trindade, and J. D. P. De Jesus, "Synthesis and characterization of tungsten trioxide powders prepared from tungstic acids," *Materials Research Bulletin*, vol. 39, no. 4-5, pp. 683–693, 2004.
- [41] J. Westerhaus, *Infrared Spectra of the Ammonium Ion in Crystals*, Royal Society of Chemistry, Cambridge, UK, 1981.
- [42] Zs. Pap, V. Danciu, Zs. Cegléd et al., "The influence of rapid heat treatment in still air on the photocatalytic activity of titania photocatalysts for phenol and monuron degradation," *Applied Catalysis B: Environmental*, vol. 101, pp. 461–470, 2011.





Hindawi

Submit your manuscripts at  
[www.hindawi.com](http://www.hindawi.com)

